nature structural & molecular biology

Structural dynamics in the gating ring of cyclic nucleotide–gated ion channels

Justin W Taraska & William N Zagotta

For ligand-gated ion channels, the binding of a ligand to an intracellular or extracellular domain generates changes in transmembrane pore-forming helices, which alters ion flow. The molecular mechanism for this allostery, however, remains unknown. Here we explore the structure and conformational rearrangements of the C-terminal gating ring of the cyclic nucleotide–gated channel CNGA1 during activation by cyclic nucleotides with patch-clamp fluorometry. By monitoring fluorescent resonance energy transfer (FRET) between membrane-resident quenchers and fluorophores attached to the channel, we detected no movement orthogonal to the membrane during channel activation. By monitoring FRET between fluorophores within the C-terminal region, we determined that the C-terminal end of the C-linker and the end of the C-helix move apart when channels open. We conclude that during channel activation, a portion of the gating ring moves parallel to the plasma membrane, hinging toward the central axis of the channel.

Ion channels regulate the flux of ions across cellular membranes[1]. Many channels are allosterically modulated by cytoplasmic domains. For example, Ca^{2+}-activated K^+ (BK) channels are activated when Ca^{2+} binds a cytoplasmic C-terminal region[2]. In addition, some transient receptor potential (TRP) channels, including TRPV1 and TRPM8, contain a cytoplasmic C-terminal domain that is responsible for the temperature-dependent activation of the channel[3]. In cyclic nucleotide–regulated channels, such as SpIH, HCN and CNG channels, the binding of ligand—cAMP or cGMP—to a cytoplasmic ligand-binding domain in the C-terminal gating ring stabilizes channel opening by 5–9 kcal mol^{-1} (ref. 4). These sensor domains provide the cell with a way to rapidly and selectively alter the activity of ion channels in response to changing cellular signals.

Recently, a structure of the cytoplasmic C-terminal region of a cyclic nucleotide–regulated channel, HCN2, has been solved by X-ray crystallography[5]. This fragment assembles into a four-fold symmetric tetramer (**Fig. 1a**), mirroring the four-fold symmetry of the pore-forming transmembrane regions. The tetrameric complex takes the form of a large ring, 52 Å in diameter and 59 Å high, with a prominent hole extending down the center. The N termini of each fragment, which in intact channels would connect to the pore-forming S6 segments, are positioned near each other at one end of the structure. The C termini reside on the opposite face of the structure. Each subunit consists of two distinct domains, the 'C-linker' and the ligand-binding domain (**Fig. 1b**). The C-linker contains six α-helices (A′–F′) separated by short loops. The ligand-binding domain follows the C-linker and is composed of four α-helices (A, P, B and C) with a β-roll situated between the A- and B-helices. A cyclic nucleotide binds inside the β-roll of each subunit and is stabilized by interactions with the C-helix[5].

To fully unravel how proteins function at the atomic level, crystallography must be coupled with other approaches. Fluorescence spectroscopy is well suited for this task. For example, measurements of FRET can determine the relative separation between two dyes within a protein[6,7]. By monitoring changes in FRET, the relative movements of domains within a protein can be determined[8]. In this study, we have used FRET to study the structure and movements of the cytoplasmic region of intact functional bovine rod CNGA1 channels in a native membrane environment. Using patch-clamp fluorometry (PCF), we were able to measure structural rearrangements within the channel, represented by site-specific fluorescence, while simultaneously monitoring channel function through current recordings[9]. We show that, contrary to current models, domains within the cytoplasmic region of the channel do not move perpendicular to the membrane during gating. We further show that a residue within the C-linker separates from the C-helix during channel opening. From these data, we infer that a portion of the cytoplasmic gating ring of CNG channels undergoes a centripetal movement during the allosteric activation of the channel by ligands.

RESULTS

Mapping channel structure with the membrane probe DPA

CNG channels are activated by the binding of cyclic nucleotides to an intracellular C-terminal ligand-binding domain[10]. Previous models have hypothesized that extensive rearrangements occur in this region during channel activation[4,11–14]. In general, conformational changes during channel gating can be broken down into two orthogonal directions, parallel and perpendicular to the membrane. We first mapped the component perpendicular to the membrane by measuring

Department of Physiology and Biophysics, Howard Hughes Medical Institute, University of Washington, Seattle, Washington 98195, USA. Correspondence should be addressed to W.N.Z. (zagotta@u.washington.edu).

Received 1 May; accepted 28 June; published online 12 August 2007; doi:10.1038/nsmb1281

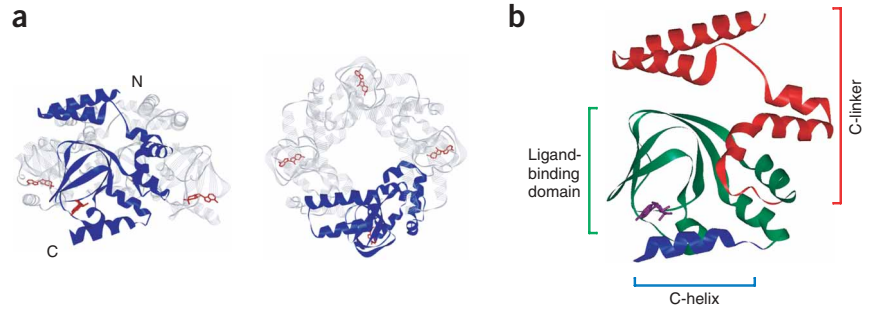

Figure 1 X-ray crystal structure of HCN2 cytoplasmic domain. (**a**) Tetrameric structure of the HCN2 cytoplasmic C-terminal region viewed from the side (left) and above (right). A single subunit is colored blue. Cyclic nucleotide is shown in red. (**b**) Domain organization of a single C-terminal region of HCN2.

FRET between dipicrylamine (DPA)—a small, negatively charged nonfluorescent membrane probe—and fluorophores attached to the channel[15]. Because the plane of the membrane is fixed, the relative distance between channel-attached fluorophores and the membrane could be monitored by following the quantity of FRET between these two probes. First, we tested whether DPA could be used as a FRET probe for ion channels tagged with green fluorescent protein (GFP).

CNGA1Δ608-GFP channels were expressed in *Xenopus laevis* oocytes and inside-out membrane patches were formed at the tips of glass micropipettes (**Supplementary Fig. 1a** online). We then measured both current and fluorescence (**Supplementary Fig. 1b**) from these isolated membrane patches. The patch shown in **Supplementary Figure 1** had 2.4 nA of current at +30 mV, which corresponds to ~2,500 channels, or ~10,000 molecules of GFP. To measure the emission spectra of the fluorophores contained in the patch, a slit was placed over the image of the patch (**Supplementary Fig. 1c**), and a spectrum was generated by reflecting the light with the grating of a spectrograph onto the chip of a CCD camera (**Supplementary Fig. 1d**). In this configuration, the horizontal dimension of the image represents wavelength whereas the vertical dimension represents position along the length of the pipette. The emission spectrum was recorded by measuring the fluorescence along a horizontal line (linescan) at the position of the patch (**Fig. 2a**, black trace). When 20 μM DPA was added to the intracellular solution, the fluorescence of GFP was substantially reduced (**Fig. 2a**, red trace). For free GFP in solution, only a minimal reduction in fluorescence (3%) was detected with the same concentrations of DPA. Evidently, GFP attached to the channel was close enough to DPA in the membrane to undergo FRET.

Because the crystallized fragment of HCN2 is only ~30% identical to CNGA1 and does not include the transmembrane domains, we wished to use FRET to determine the location of the equivalent domains in the C-terminal region of intact CNGA1 channels. The absorbance spectrum of DPA (**Supplementary Fig. 2** online, dotted black line) overlaps in decreasing magnitude with the emission spectra of GFP (blue), Alexa 488 (green) and Alexa 568 (magenta). Thus, DPA can be used as a FRET acceptor for all three of these dyes and can be paired with each to report distances over a wide range. Three fluorescently tagged channel constructs were used in these experiments: (i) GFP attached to the distal C terminus (CNGA1-GFP), (ii) GFP attached after residue Asp608 of the C-helix of the ligand-binding domain (CNGA1Δ608-GFP) and (iii) a construct where a native cysteine in the C-linker present in an otherwise cysteine-free channel was labeled with a thiol-reactive dye ($CNGA1_{Cys481}$-Alexa-488 or $CNGA1_{Cys481}$-Alexa-568) (**Fig. 2b**). Unlike labeling proteins with GFP, whose fluorescence is specific to the channel, labeling proteins with thiol-reactive fluorophores *in vivo* can result in background fluorescence from nonspecific labeling of endogenous cysteines[16]. We were able to specifically label residue Cys481 with thiol-reactive dyes because this residue has been shown to be reactive to cysteine modification only when the channel is open[9,16–18]. Thus, background cysteines first can be blocked by covalent modification with the nonfluorescent thiol-reactive molecule *N*-ethylmaleimide (NEM) when the channel is closed. The channel then can be opened with ligand, and Cys481 can be labeled specifically with fluorophore[16].

Different FRET efficiencies, calculated from the quantity of donor quenching, were observed between DPA and the three channel constructs: for CNGA1-GFP, 30.5% ± 3%, $n = 7$; for CNGA1Δ608-GFP, 43.7% ± 2.4%, $n = 8$; and for $CNGA1_{Cys481}$-Alexa-488, 66.3% ± 2%, $n = 7$ (**Fig. 2c**). Moreover, when the fluorophore at position Cys481 was switched from Alexa 488 to Alexa 568, a fluorophore whose emission spectrum overlaps to a lesser degree with DPA's absorption spectrum, FRET was less pronounced (47% ± 2.5%, $n = 7$), which further confirms that DPA acted as a FRET acceptor in these experiments (**Fig. 2c**). From these data, we conclude that the C-linker is closest to the membrane, followed by the C-helix and the distal C terminus. This orientation is consistent with a position for the fragment of HCN2 solved by crystallography such that the N terminus of each fragment is nearest to the membrane, where it would connect to the S6 transmembrane segment in full-length channels. The C-linker, C-helix and distal C terminus, respectively, each extend progressively further into the cytoplasm.

FRET is sensitive to movement

In addition to using FRET to map the static position of residues in closed channels, we were interested in determining whether FRET could be used to detect conformational rearrangements within the

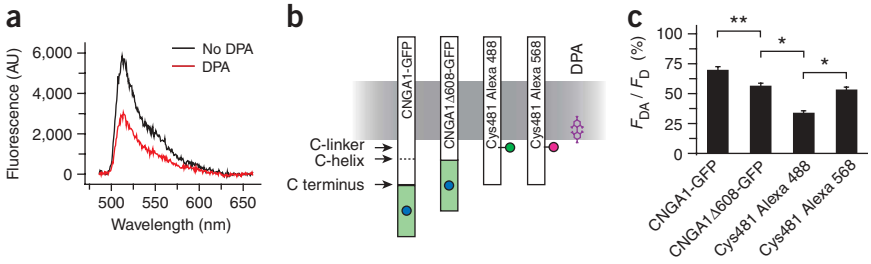

Figure 2 FRET between fluorescently labeled ion channels and the membrane probe, DPA, measured with patch-clamp fluorometry. (**a**) Linescan measurement of CNGA1Δ608-GFP spectrum before (black) and after (red) addition of 20 μM DPA at 0 mV. AU, arbitrary units. (**b**) Cartoon of CNGA1 channel constructs, with GFP as a green rectangle and fluorophores as circles. (**c**) Steady-state quenching of channel fluorescence by DPA at 0 mV. Plotted is the average fluorescence remaining after addition of quencher. Error bars show s.e.m. $^{**}P = 0.004$; $^{*}P < 0.00002$ (Student's *t*-test).

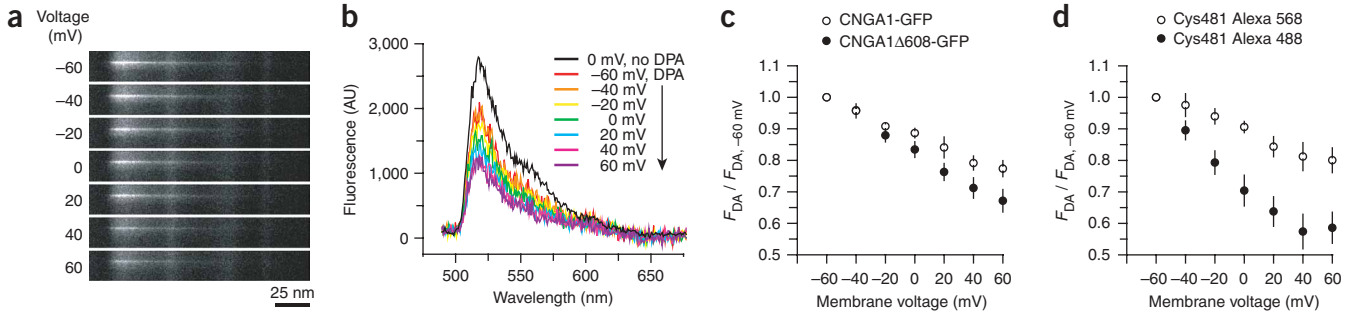

Figure 3 FRET between fluorescent channels and the membrane probe, DPA, is sensitive to movement. (**a**,**b**) Spectral images (**a**) and linescans (**b**) of a patch expressing CNGA1Δ608-GFP in the presence of 20 μM DPA at different membrane voltages. The fluorescence of the patch before the addition of DPA is shown as a black line in **b**. AU, arbitrary units. (**c**) Plot of fluorescence for channels labeled with GFP at the extreme C terminus (open circles) or after the C-helix (closed circles) in the presence of DPA at different voltages. (**d**) Voltage dependence of FRET between Cys481 channels labeled with either Alexa 488 (closed circles) or Alexa 568 (open circles) in the presence of DPA. Error bars in **c** and **d** show ± s.e.m.

channel. To confirm that our FRET measurements could report changes in distance between the channel and the membrane, we artificially shifted the position of DPA in the membrane with voltage[15,19]. DPA is negatively charged and will move from the outer to the inner leaflet of the membrane when the voltage is shifted to positive potentials[19,20]. Thus, FRET between GFP and DPA should become greater at positive potentials. As expected, the patch became dimmer as the voltage was stepped to more positive potentials, indicating that FRET increased as DPA moved closer to GFP (**Fig. 3a,b**). For all three fluorophore positions tested—at the end of the C terminus, after the C-helix, and at the end of the C-linker (Cys481)—moving DPA to the inner membrane robustly increased FRET (**Fig. 3c,d**). These results demonstrate that DPA can be used to reliably detect movement between these positions within the channel and the membrane.

No orthogonal movement during gating

Previous models have predicted movement of the cytosolic region of CNG channels perpendicular to the membrane when the channel binds ligand and opens[4,11–14]. We explored this idea by measuring FRET between the channel and DPA in both the closed and open states of the channel. The spectra of a patch containing CNGA1Δ608-GFP quenched by DPA in the absence (**Fig. 4a**, black line) or presence (red line) of 2 mM cGMP show no change in FRET between the closed and open states. For all three fluorophore positions tested—at the end of the C terminus, after the C-helix, and at the end of the C-linker (Cys481)—FRET during channel opening was not substantially different from the results with the control constructs, a membrane-anchored farnesylated GFP (EGFP-F)[19] and a cysteine-free CNGA1 (**Fig. 4b**). We are confident that the lack of FRET changes seen in these experiments is not due to the sensitivity of our measurements, as we can detect large FRET changes when the acceptor is artificially moved with voltage (see **Fig. 3**). These data demonstrate that these three domains in the channel do not move substantially perpendicular to the plane of the membrane during channel opening.

Intramolecular FRET measurements in the gating ring

Given that no movement was detected between the C-terminal region and the membrane, we next asked whether domains within the C-terminal region move relative to one another during channel activation. To test this idea, we created channels that contained both GFP at the end of the C-helix and Cys481 at the end of the C-linker ($CNGA1_{Cys481}$Δ608-GFP, **Fig. 5a**). We then measured FRET between GFP and this cysteine modified with the fluorophore Alexa 568, to track rearrangements within the C-terminal region of the channel. The spectral overlap of the two fluorophores (**Fig. 5b**) results in a calculated Förster radius[6] (R_0) of 54 Å, which is similar to the distance between Cys481 and the chromophore of GFP (58 Å) predicted by the model shown in **Figure 5a** (see below). These two fluorophores, therefore, should be positioned at a favorable distance for FRET.

Supplementary Fig. 3a–c online shows the fluorescence image and spectrum of a patch expressing the construct $CNGA1_{Cys481}$Δ608-GFP. As in **Figure 2**, to specifically label the channel with a thiol-reactive fluorophore, we used NEM to block both endogenous background cysteines in the patch and GFP-Cys48, the single reactive cysteine in GFP[21,22], when the channel was closed. The channel was then opened with ligand and Cys481 was labeled with fluorophore. **Supplementary Fig. 3d,e** shows the image and spectrum of this patch after labeling of Cys481 with Alexa 568 maleimide in the open state. The patch became brighter, presumably owing to the addition of new fluorophores to the channel. The introduction of Alexa 568 had two effects on the spectrum: (i) the addition of a red component, corresponding to the fluorescence of Alexa 568, and (ii) a decrease in the intensity of the GFP peak (compare **Supplementary Fig. 3c,e**). This also can be seen in linescan measurements (**Fig. 5c**). Averaged over a number

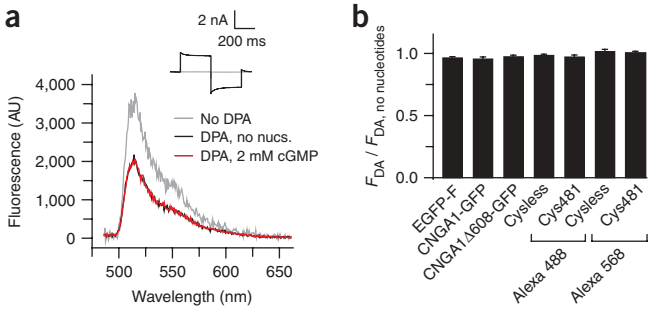

Figure 4 FRET between the channel and DPA does not change during ligand activation. (**a**) Spectra of CNGA1Δ608-GFP in the presence (red) or absence (black) of 2 mM cGMP. The fluorescence of the patch before the addition of DPA is shown as a gray line. Inset shows current in the presence of 2 mM cGMP. AU, arbitrary units. (**b**) Plot of state-dependent changes in fluorescence in the presence of 2 mM cGMP. No appreciable change in FRET during channel opening, compared with controls, was measured at all positions. Error bars show ± s.e.m.

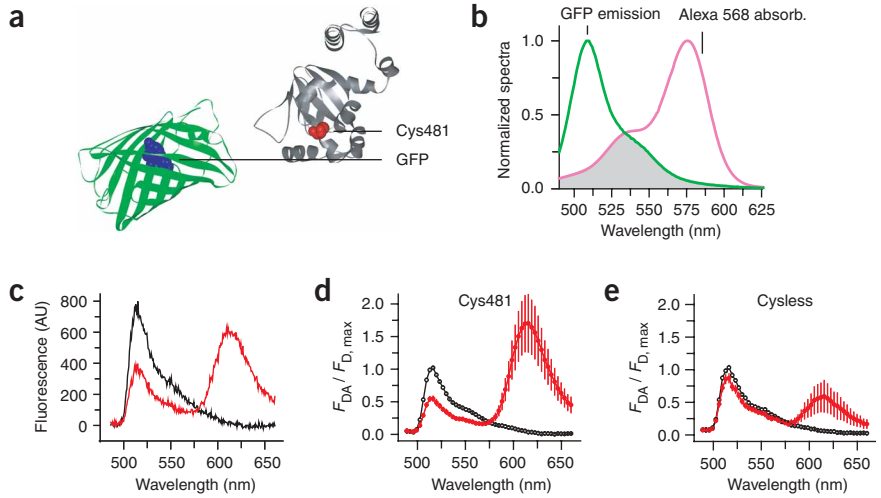

Figure 5 Two-color labeling of channels with GFP and Alexa 568. (**a**) Model of the C-terminal region of CNGA1Δ608 fused to GFP. Cys481 is shown in red. (**b**) Spectral overlap (gray) between the emission of GFP (green line) and absorbance of Alexa 568 (magenta line). (**c**) Linescan of a patch containing $CNGA1_{Cys481}$Δ608-GFP before (black) and after (red) labeling Cys481 with Alexa 568. AU, arbitrary units. (**d**) Average fluorescence spectrum of patches containing $CNGA1_{Cys481}$Δ608-GFP channels blocked with NEM, before (black) and after (red) labeling of Cys481 with Alexa 568. (**e**) Average traces of patches containing cysteine-free (Cysless) channels ($CNGA1_{Cysless}$Δ608-GFP) blocked with NEM, before (black) and after (red) labeling with Alexa 568. In **d** and **e**, error bars show ± s.e.m.

of patches, the decrease in the fluorescence of GFP after Alexa 568 labeling was 46% ± 4% (n = 6; **Fig. 5d**). In a control experiment, patches containing cysteine-free CNG channels ($CNGA1_{Cysless}$Δ608-GFP) blocked with NEM and then labeled with Alexa 568 maleimide showed minimal decreases in GFP fluorescence (14% ± 6%, n = 4) and only a small amount of nonspecific background labeling (**Fig. 5e**). Thus, the fluorophore attached to Cys481 was close enough to undergo FRET with a GFP molecule attached to the end of the C-helix.

Movements detected during the allosteric transition

We next asked whether residue Cys481 moves in relation to the C-helix when the channel opens. **Figure 6a** shows current traces in the presence of 2 mM cGMP (blue) or 16 mM cAMP (red) in a patch containing $CNGA1_{Cys481}$Δ608-GFP labeled at Cys481 with Alexa 568. Notably, the spectrum of dual-labeled channels changed in the presence of activating ligand (**Fig. 6b**). When the channel was opened, the GFP fluorescence increased while the Alexa 568 fluorescence decreased. This also can be seen in the point-by-point change in fluorescence between the open and closed state (**Fig. 6c**). It is evident from this trace that a reciprocal change occurred between the fluorescence intensity of the donor (GFP) and the fluorescence intensity of the acceptor (Alexa 568). On average, the GFP fluorescence became 12.6% ± 1% brighter (**Fig. 6d**, n = 5), whereas the Alexa 568 fluorescence was diminished by 7.4% ± 2% (**Fig. 6d**). These data show that FRET was less efficient in the open state.

To verify that the changes in FRET were not due to changes in the orientations of the two probes, we measured anisotropy. The anisotropy of $CNGA1_{Cys481}$ channels labeled at Cys481 with Alexa 568 was measured in the absence or presence of activating ligand. The steady-state anisotropy values were small and identical (no nucleotide, 0.13 ± 0.01; 2 mM cGMP, 0.13 ± 0.01; n = 5). These results, along with the low anisotropy values of CNGA1Δ608-YFP channels previously reported[23], indicate that the change in FRET we observed is not the consequence of a change in the orientation of the probes but instead results from a change in distance. This change in FRET suggests that the two fluorophores move 2.5 Å apart during channel activation.

Notably, the FRET change we measured was related to the fraction of open channels, not the fraction of channels bound by ligand. Saturating concentrations of the partial agonist cAMP produced 39% ± 5% of the current and approximately half of the FRET change that was induced by cGMP (**Fig. 6d,e**). These data suggest that the rearrangement detected by FRET between Cys481 and GFP attached to the C-helix reflects a change closely coupled to channel opening and

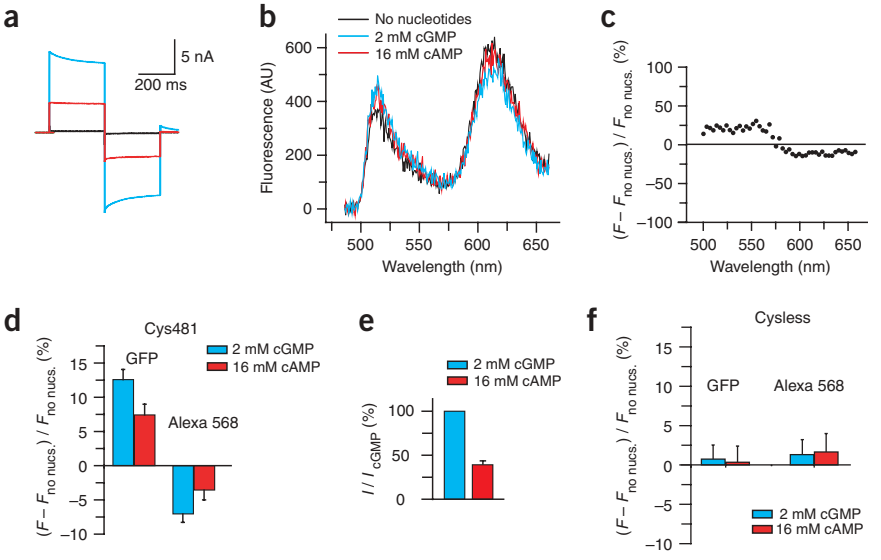

Figure 6 The C-helix and residue Cys481 separate during ligand activation. (**a**,**b**) Current traces (**a**) and spectra (**b**) of $CNGA1_{Cys481}$Δ608-GFP labeled with Alexa 568, imaged in the presence of no nucleotides (black), 2 mM cGMP (blue) or 16 mM cAMP (red). AU, arbitrary units. (**c**) Change in fluorescence between experiments with no nucleotides and with 2 mM cGMP, for the patch used in **b**. (**d**) Plot of donor and acceptor fluorescence changes for $CNGA1_{Cys481}$Δ608-GFP labeled with Alexa 568 during the addition of 2 mM cGMP or 16 mM cAMP. (**e**) Current activated by 2 mM cGMP (blue) or 16 mM cAMP (red) for patches used in **d**. (**f**) Plot of donor and acceptor fluorescence changes for $CNGA1_{Cysless}$Δ608-GFP labeled with Alexa 568 during the addition of 2 mM cGMP (blue) or 16 mM cAMP (red). Error bars in **d** and **f** show ± s.e.m.

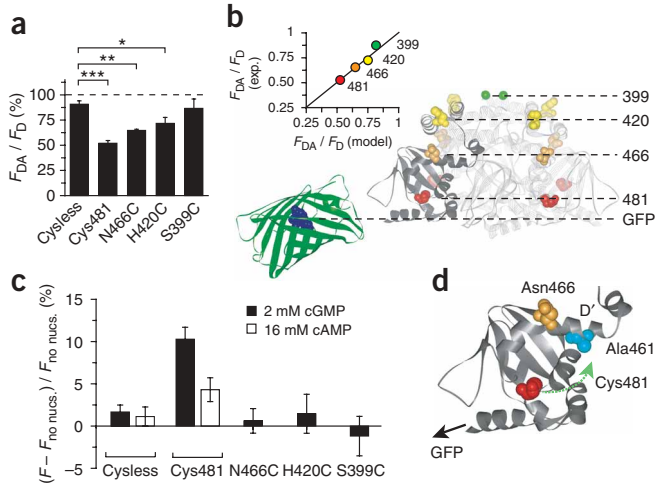

Figure 7 FRET measurements between GFP and residues throughout the C-terminal region of CNGA1. (**a**) Steady-state quenching of GFP by residues labeled with Alexa 568 in closed channels. Plotted is the average fluorescence remaining after modification. Error bars show s.e.m. $***P < 0.00001$; $**P = 0.0008$; $*P = 0.006$ (Student's *t*-test). (**b**) Position of residues labeled with Alexa 568. Green, Ser399; yellow, His420; orange, Asn466; red, Cys481. GFP is positioned at the location predicted by the quenching values shown in **a**. Inset compares the expected quenching values from the model with the experimental data corrected for background, for each residue. (**c**) State-dependent changes in FRET between GFP and residues Cys481, N466C, H420C and S399C labeled with Alexa 568. Error bars in **a** and **c** show ± s.e.m. (**d**) Model for the movement of Cys481 (red) away from the C-helix and toward the central cavity of the channel.

not ligand binding. No change in FRET was detected for the control construct $CNGA1_{cysless}\Delta608$-GFP labeled with Alexa 568 when the channel was opened with ligand (**Fig. 6f**).

FRET measurements throughout the gating ring

Do any other residues in the cytoplasmic region change position relative to the C-helix when the channel opens? We tested this by introducing individual cysteines throughout the C-linker. Unlike Cys481, other residues are not protected from thiol modification in a state-dependent manner. Thus, we were not able to block these patches with NEM. Without blocking, thiol-reactive dyes are free to react with endogenous background cysteines and GFP Cys48, the reactive cysteine in GFP. To circumvent these problems, we took two steps. First, Cys48 of GFP was mutated to valine. Second, we reasoned that if background cysteines in the patch were beyond the FRET range of GFP, fluorophores attached to background cysteines would not substantially quench the GFP fluorescence. This was indeed the case (**Fig. 7a**). Labeling with Alexa 568 produced little change in the GFP fluorescence of patches containing $CNGA1_{Cysless}\Delta608$-GFP(C48V) (9.2% ± 3%, $n = 14$). Thus, even though labeling background cysteines produced a large amount of the acceptor fluorescent signal, we still could use donor-quenching measurements as a readout for channel-specific FRET.

We introduced cysteines into $CNGA1_{Cysless}\Delta608$-GFP(C48V) at three positions, giving a total of four channel constructs, each with a unique single cysteine residue per subunit: S399C, H420C, N466C and Cys481. When the patches were reacted with Alexa 568 maleimide, little donor quenching was observed for $CNGA1_{Cysless}\Delta608$-GFP(C48V), yet substantial quenching was observed for three of the cysteine mutants (**Fig. 7a**). FRET between Cys481 labeled with Alexa 568 and GFP(C48V) measured by donor quenching was again large (48% ± 3%, $n = 9$), essentially identical to the amount observed in $CNGA1_{Cys481}\Delta608$-GFP channels (with wild-type GFP) blocked with NEM before dye labeling. Residues that we predicted to be progressively farther from the C-helix produced decreasing amounts of donor quenching (**Fig. 7a**,**b**). Indeed, the residue that we presumed to be the closest to the membrane, at position 399, showed very little quenching compared with the control (**Fig. 7a**).

Because FRET efficiencies can be used to calculate the distance between two fluorophores, we were able to model the position of the GFP in relation to the C-terminal region of the channel. On the basis of the crystal structure of HCN2, distances were calculated between each labeled residue in the channel complex and each possible location of the GFP. We then determined the GFP location that produced the best fit, in a least-squares analysis, between the observed quenching efficiencies and those predicted from the crystal structure. This analysis positions the chromophore of GFP 63 Å from the tip of the C-helix (**Fig. 7b**). The modeled distances between the GFP and the nearest cysteine residue from the four channel subunits are as follows: 94 Å (S399C, same subunit), 74 Å (H420C, adjacent subunit), 65 Å (N466C, same subunit) and 58 Å (Cys481, same subunit) (**Fig. 7b**). The FRET efficiencies calculated from this structural model closely match our experimental data (**Fig. 7b**, inset).

Because we were able to detect FRET changes between Cys481 and GFP during channel opening (**Fig. 6**), we next asked whether other cysteine residues moved relative to the GFP during the allosteric transition. FRET changes were measured again in Cys481 patches (this time in unblocked patches containing GFP(C48V)). Changes in donor quenching when the channel was opened with 2 mM cGMP (10.3% ± 1.4%, $n = 9$) were similar to those measured in $CNGA1_{Cys481}\Delta608$-GFP (**Fig. 7c**). The fluorescence change induced by the partial agonist cAMP was again about half (4.3% ± 1.4%, $n = 9$) of that seen with the full agonist cGMP. Notably, all other cysteines tested—N466C (0.6% ± 1.5%, $n = 4$), H420C (1.5% ± 2.3%, $n = 5$) and S399C (–1.2% ± 2.3%, $n = 3$)—did not show any marked change in FRET between the open and closed states of the channel (**Fig. 7c**). Because these positions are located at increasing distances from the GFP and thus have decreasing steady-state FRET efficiencies (see **Fig. 7a**), an increasingly large change in distance would have been needed to produce changes in FRET similar to those seen with Cys481. Nonetheless, a change in fluorescence of ~2%, which would equate to a movement of 0.7 Å for N466C, 1.1 Å for H420C and 11.7 Å for S399C, would have been detected. In summary, our results suggest that although many points in the C-linker remain relatively stationary, the loop containing Cys481 moves away from the tip of the C-helix, probably moving toward the central axis of the channel during the allosteric transition (**Fig. 7d**).

DISCUSSION

Here we simultaneously measured site-specific fluorescent signals and ionic currents to map the structure and movements of domains within the CNGA1 channel during ligand activation. We detected no movement of three positions within the cytoplasmic C-terminal region relative to the membrane. We did, however, detect conformational changes between the end of the ligand-binding domain and the C-linker. From these data, we conclude that this region of the C-linker moves away from the C-helix but parallel to the membrane during channel activation. The amount of FRET we measured was proportional to the fraction of open channels, suggesting that this

movement occurs during the conformational change responsible for channel opening, not ligand binding. This can be inferred because saturating concentrations of both cGMP and cAMP were used, yet the full agonist, cGMP, produced a much larger change in FRET than did the partial agonist, cAMP.

Ion channels that are regulated by cyclic nucleotides share structurally similar C-terminal regions[4]. Although each channel subtype is modulated to a different degree by cyclic nucleotides, the individual domains probably behave in mechanistically similar ways. Models of how these cytoplasmic domains regulate the opening of cyclic nucleotide–regulated channels have been proposed[4]. For example, in HCN channels, the C-terminal region has been suggested to act as an autoinhibitor of channel gating[24]. Similar mechanisms have been proposed for other cyclic nucleotide–regulated channels, including CNGA1 channels and SpIH channels[11,25]. Indeed, past work has suggested that a large conformational change in this region might occur to release the autoinhibition during ligand activation[11–14]. Our data do not support such a large conformational change. Instead, our work suggests that movements within the C-linker are probably subtle, involving limited structural rearrangements. Indeed, the primary movement we detected was a separation of Cys481 from the end of the C-helix. Cys481 resides in a loop situated between the ligand-binding domain and the α-helices of the C-linker. Activation of the channel causes Cys481 to move toward the central axis of the channel. This centripetal movement is consistent with previous work suggesting that residue Cys481 and residue Ala461 on the D′ helix (see **Fig. 7d**) are closer together in the open state[16]. In summary, our evidence suggests that during the allosteric opening of the channel, the loop containing Cys481 moves parallel to the plasma membrane, hinging away from the C-helix and toward the stationary D′-helix. Analogous parallel movements have been proposed for Ca^{2+}-activated K^+ channels[26,27]. However, given the limited points of measurement, the large working distance for FRET (30–70 Å) and the relatively large size of our probes, we were unable to resolve the complete conformational rearrangements in the C-linker during channel gating. Other fluorescence and spectroscopic techniques will probably fill this gap, providing a deeper understanding of the discrete conformational changes that occur in the channel's structure[16,28,29].

The accumulation of crystal structures has provided a wealth of detail about the atomic organization of ion channels and other membrane proteins. Crystal structures, however, are snapshots of only one conformation of a protein. Indeed, it is rare for a membrane protein to be crystallized in different conformations. Furthermore, it is difficult to assign structures to functional states of the protein. Whether a crystal structure accurately represents the conformation of the protein in its native membrane environment is also exceptionally difficult to ascertain. Fluorescence holds the promise of bridging the gap between functional and structural methods in protein biophysics. For understanding how proteins shift from one state to another, moving between short-lived and unstable transition states, methods that can detect dynamic changes in protein structure will provide invaluable information. We have developed such a method for ion channels, one that allows simultaneous functional and structural measurements to map the dynamic rearrangements directly involved in the allosteric activation of these membrane proteins.

METHODS

Molecular biology. CNGA1 channel–GFP fusions were created by cloning the open reading frame (ORF) of EGFP (Clontech) onto the distal C terminus of the CNGA1 channel[30] to create CNGA1-GFP, or after amino acid residue Asp608 to create CNGA1Δ608-GFP. For all other constructs, the CNGA1 channel with all seven endogenous cysteines removed was used as a template for mutagenesis[14]. Cysteines were introduced at positions 399, 420, 466 and 481 using PCR as described[31]. To remove the reactive cysteine from EGFP, PCR mutagenesis was used to introduce the C48V mutation. All mutations were confirmed by sequencing. All constructs were created in the pGEMHE oocyte expression vector. RNA was prepared with the mMessage machine kit (Ambion) and injected into *Xenopus laevis* oocytes as described[31].

Electrical recording and solutions. Current was recorded on inside-out patches[32] formed at the tip of 200- to 800-kΩ glass pipettes and measured with an Axopach 200A amplifier (Axon Instruments) using PULSE acquisition software (HEKA electronik). Patches were perfused using a rapid solution changer (BioLogic). The solutions in the pipette and bath were as follows: 130 mM NaCl, 0.2 mM EDTA and 3 mM HEPES (pH 7.2), with 2 mM cGMP or 16 mM cAMP added to the perfusion solution as indicated. For cysteine modification, NEM (Sigma) or Alexa 568 C5 maleimide (Invitrogen) was dissolved in bath solution (with or without nucleotides) and perfused onto the patch. A stock solution of dipicrylamine (City Chemicals) was made fresh from powder before each experiment and dissolved in perfusion solutions to a final concentration of 20 μM.

Optical recording and analysis. Optical recordings of inside-out membrane patches were performed on a Nikon Eclipse TE2000-E with a ×60 1.4 NA Plan Apo oil-immersion objective (Nikon). GFP, Alexa 488 and Alexa 568 were excited with the 488-nm laser line from an argon laser (Spectra Physics) coupled through an optical fiber to the total internal reflection (TIRF) module of the microscope. The beam passed through an excitation filter (Chroma Z488/5) and was directed through the center of the objective with a dichroic mirror (Chroma Z488rdc). Emission light was collected through a long-pass filter (Chroma HQ495lp) and reflected onto the grating of a spectrograph (Acton MicroSpec 2150i). Light was recorded by a Cascade 512B intensified CCD camera (Roper Scientific). For spectroscopic recordings, a slit was placed over the image of the patch and the emission was directed onto a grating (300/500 blazing) to create an image of the spectrum. In this configuration, the abscissa represents wavelength and the ordinate represents the spatial dimension along the axis of the pipette. Pixels were binned 2 × 2 and acquired with a 250-ms exposure. Each pixel spanned a wavelength of 0.67 nm. For spatial imaging, the spectrograph grating was placed at the zero-order position and the spatial filter was removed. In this mode, one pixel was 0.48 μm. Images were analyzed with Metamorph software (Molecular Devices). Spectra were analyzed by measuring linescans across the region corresponding to the patch. Spectra were background-corrected by subtracting a linescan of the nonfluorescent region directly above the patch. For quenching measurements, fluorescence values were averaged over the 50 pixels after the peak of the spectrum. To measure changes in fluorescence, average values were calculated from the ten pixels surrounding the peak spectrum of each fluorophore. Traces were normalized to the ten pixels surrounding the average peak of the spectrum. All errors shown are s.e.m. Student's *t*-test was used to test for significance, defined as $P \leq 0.05$ (OriginLab).

Measurements of anisotropy. Anisotropy was measured on inside-out membrane patches containing channels labeled with fluorophores as described[23]. Measurements were made on a Nikon Diaphot 300 with both a ×40 0.5 NA objective and a ×10 0.25 NA objective. Alexa 568 was excited with a xenon light source (Opti Quip) that passed through an excitation filter (Chroma HQ510/40) and was directed onto the sample with a dichroic mirror (Chroma 540dclp). Emission light was collected through a long-pass emission filter (Chroma HQ545lp). Images were recorded with a Micromax CCD camera (Roper Scientific). An excitation polarizer was positioned directly in front of the excitation filter, and two emission polarizers, one in a parallel (||) and the other in a perpendicular (⊥) orientation, were positioned directly below the emission filter in a sliding holder. The steady-state anisotropy values were calculated using the equation[8] $A = (I_{||} - GI_{\perp})/(I_{||} + 2GI_{\perp})$. The intrinsic polarization properties of the optical system were determined by measuring the anisotropy of tetramethylrhodamine methyl ester (TMRM; Invitrogen) dissolved in glycerol, which has an anisotropy of 0.38 (ref. 33). From these measurements, a *G*-factor of between 0.815 and 0.865 was used to calibrate channel anisotropy values.

FRET calculations and structural modeling. FRET efficiencies (E) were calculated from the equation $E = 1 - F_{DA}/F_D$, where F_{DA} is the fluorescence of the donor in the presence of acceptor and F_D is the fluorescence of the donor without acceptor[8]. E was used to calculate intramolecular distances between two fluorophores with the relationship $R = R_0((1/E) - 1)^{-6}$, where R is the distance between the two dyes and R_0 is the Förster distance, assuming an orientation factor κ^2 of 2/3 (ref. 8). To calculate the total E between one donor and four acceptors, the following equation was used, where r_1, r_2, r_3 and r_4 are the distances to the four individual acceptors[8,34].

$$E_{total} = \frac{R_0^6\left(\frac{1}{r_1^6}+\frac{1}{r_2^6}+\frac{1}{r_3^6}+\frac{1}{r_4^6}+\frac{1}{r_B^6}\right)}{1 + R_0^6\left(\frac{1}{r_1^6}+\frac{1}{r_2^6}+\frac{1}{r_3^6}+\frac{1}{r_4^6}+\frac{1}{r_B^6}\right)}$$

A correction for background was made by adding a fifth distance term (r_B) that is proportional to the amount of background quenching observed. A homology model of the C-terminal region of CNGA1 was created on the basis of the HCN2 crystal structure[5] using the SWISS-MODEL server at http://swissmodel.expasy.org//SWISS-MODEL.html as described[35,36]. From this model, the Cartesian coordinates were determined for the β-carbons of the residues His420, Asn466 and Cys481 from all four subunits. The coordinates of Ser399 were estimated by finding the equivalent positions in the crystal structure of KV1.2 (refs. 35,37) docked to the HCN2 structure. Using these spatial coordinates, the theoretical E-values were calculated for FRET between each of the four residues, along with a test position for the chromophore of GFP. The solver function of Excel (Microscoft) was used to identify the position of GFP that yielded the best fit (by the least-squares method) between the predicted and experimental E-values for all residues tested. All structural models were drawn using ViewerPro 4.2 (Accelrys).

Note: Supplementary information is available on the Nature Structural & Molecular Biology website.

ACKNOWLEDGMENTS

We thank H. Utsugi, S. Cunnington and G. Sheridan for technical assistance, E.R. Liman (University of Southern California) for the pGEMHE oocyte expression vector, R.T. Moon (University of Washington) for the plasmid encoding EGFP-F, W. Almers, K. Craven, G. Flynn, A. Merz, M. Puljung and N. Shuart for comments on the manuscript, and L. Islas for stimulating discussions. This work was supported by the Howard Hughes Medical Institute, a grant from the National Eye Institute of the US National Institutes of Health (EY10329) to W.N.Z. and a postdoctoral fellowship from the Jane Coffin Childs Foundation to J.W.T.

COMPETING INTERESTS STATEMENT

The authors declare no competing financial interests.

Published online at http://www.nature.com/nsmb
Reprints and permissions information is available online at http://npg.nature.com/reprintsandpermissions

1. Hille, B. *Ion Channels of Excitable Membranes* (Sinauer, Sunderland, Massachusetts, USA, 2001).
2. Schreiber, M., Yuan, A. & Salkoff, L. Transplantable sites confer calcium sensitivity to BK channels. *Nat. Neurosci.* **2**, 416–421 (1999).
3. Brauchi, S., Orta, G., Salazar, M., Rosenmann, E. & Latorre, R. A hot-sensing cold receptor: C-terminal domain determines thermosensation in transient receptor potential channels. *J. Neurosci.* **26**, 4835–4840 (2006).
4. Craven, K.B. & Zagotta, W.N. CNG and HCN channels: two peas, one pod. *Annu. Rev. Physiol.* **68**, 375–401 (2006).
5. Zagotta, W.N. *et al.* Structural basis for modulation and agonist specificity of HCN pacemaker channels. *Nature* **425**, 200–205 (2003).
6. Selvin, P.R. Fluorescence resonance energy transfer. *Methods Enzymol.* **246**, 300–334 (1995).
7. Vogel, S.S., Thaler, C. & Koushik, S.V. Fanciful FRET. *Sci. STKE* **2006**, re2 (2006).
8. Lakowicz, J.R. *Principles of Fluorescence Spectroscopy* (Plenum, New York, 1999).
9. Zheng, J. & Zagotta, W.N. Gating rearrangements in cyclic nucleotide-gated channels revealed by patch-clamp fluorometry. *Neuron* **28**, 369–374 (2000).
10. Zagotta, W.N. & Siegelbaum, S.A. Structure and function of cyclic nucleotide-gated channels. *Annu. Rev. Neurosci.* **19**, 235–263 (1996).
11. Craven, K.B. & Zagotta, W.N. Salt bridges and gating in the COOH-terminal region of HCN2 and CNGA1 channels. *J. Gen. Physiol.* **124**, 663–677 (2004).
12. Johnson, J.P., Jr & Zagotta, W.N. Rotational movement during cyclic nucleotide-gated channel opening. *Nature* **412**, 917–921 (2001).
13. Hua, L. & Gordon, S.E. Functional interactions between A′ helices in the C-linker of open CNG channels. *J. Gen. Physiol.* **125**, 335–344 (2005).
14. Matulef, K., Flynn, G.E. & Zagotta, W.N. Molecular rearrangements in the ligand-binding domain of cyclic nucleotide-gated channels. *Neuron* **24**, 443–452 (1999).
15. Chanda, B., Asamoah, O.K., Blunck, R., Roux, B. & Bezanilla, F. Gating charge displacement in voltage-gated ion channels involves limited transmembrane movement. *Nature* **436**, 852–856 (2005).
16. Islas, L.D. & Zagotta, W.N. Short-range molecular rearrangements in ion channels detected by tryptophan quenching of bimane fluorescence. *J. Gen. Physiol.* **128**, 337–346 (2006).
17. Gordon, S.E., Varnum, M.D. & Zagotta, W.N. Direct interaction between amino- and carboxyl-terminal domains of cyclic nucleotide-gated channels. *Neuron* **19**, 431–441 (1997).
18. Brown, R.L., Snow, S.D. & Haley, T.L. Movement of gating machinery during the activation of rod cyclic nucleotide-gated channels. *Biophys. J.* **75**, 825–833 (1998).
19. Chanda, B. *et al.* A hybrid approach to measuring electrical activity in genetically specified neurons. *Nat. Neurosci.* **8**, 1619–1626 (2005).
20. Fernandez, J.M., Taylor, R.E. & Bezanilla, F. Induced capacitance in the squid giant axon. Lipophilic ion displacement currents. *J. Gen. Physiol.* **82**, 331–346 (1983).
21. Inouye, S. & Tsuji, F.I. Evidence for redox forms of the *Aequorea* green fluorescent protein. *FEBS Lett.* **351**, 211–214 (1994).
22. Ostergaard, H., Henriksen, A., Hansen, F.G. & Winther, J.R. Shedding light on disulfide bond formation: engineering a redox switch in green fluorescent protein. *EMBO J.* **20**, 5853–5862 (2001).
23. Zheng, J., Varnum, M.D. & Zagotta, W.N. Disruption of an intersubunit interaction underlies Ca^{2+}-calmodulin modulation of cyclic nucleotide-gated channels. *J. Neurosci.* **23**, 8167–8175 (2003).
24. Wainger, B.J., DeGennaro, M., Santoro, B., Siegelbaum, S.A. & Tibbs, G.R. Molecular mechanism of cAMP modulation of HCN pacemaker channels. *Nature* **411**, 805–810 (2001).
25. Vemana, S., Pandey, S. & Larsson, H.P. S4 movement in a mammalian HCN channel. *J. Gen. Physiol.* **123**, 21–32 (2004).
26. Ye, S., Li, Y., Chen, L. & Jiang, Y. Crystal structures of a ligand-free MthK gating ring: insights into the ligand gating mechanism of K^+ channels. *Cell* **126**, 1161–1173 (2006).
27. Jiang, Y. *et al.* Crystal structure and mechanism of a calcium-gated potassium channel. *Nature* **417**, 515–522 (2002).
28. Popovych, N., Sun, S., Ebright, R.H. & Kalodimos, C.G. Dynamically driven protein allostery. *Nat. Struct. Mol. Biol.* **13**, 831–838 (2006).
29. Cordero-Morales, J.F. *et al.* Molecular determinants of gating at the potassium-channel selectivity filter. *Nat. Struct. Mol. Biol.* **13**, 311–318 (2006).
30. Kaupp, U.B. *et al.* Primary structure and functional expression from complementary DNA of the rod photoreceptor cyclic GMP-gated channel. *Nature* **342**, 762–766 (1989).
31. Gordon, S.E. & Zagotta, W.N. A histidine residue associated with the gate of the cyclic nucleotide-activated channels in rod photoreceptors. *Neuron* **14**, 177–183 (1995).
32. Hamill, O.P., Marty, A., Neher, E., Sakmann, B. & Sigworth, F.J. Improved patch-clamp techniques for high-resolution current recording from cells and cell-free membrane patches. *Pflugers Arch.* **391**, 85–100 (1981).
33. Cha, A. & Bezanilla, F. Structural implications of fluorescence quenching in the Shaker K+ channel. *J. Gen. Physiol.* **112**, 391–408 (1998).
34. Wolber, P.K. & Hudson, B.S. An analytic solution to the Forster energy transfer problem in two dimensions. *Biophys. J.* **28**, 197–210 (1979).
35. Flynn, G.E. & Zagotta, W.N. Conformational changes in S6 coupled to the opening of cyclic nucleotide-gated channels. *Neuron* **30**, 689–698 (2001).
36. Guex, N. & Peitsch, M.C. SWISS-MODEL and the Swiss-PdbViewer: an environment for comparative protein modeling. *Electrophoresis* **18**, 2714–2723 (1997).
37. Long, S.B., Campbell, E.B. & Mackinnon, R. Crystal structure of a mammalian voltage-dependent Shaker family K^+ channel. *Science* **309**, 897–903 (2005).